

ALMA MATER STUDIORUM · UNIVERSITÀ DI
BOLOGNA

Dipartimento di Fisica e Astronomia “Augusto Righi”
Corso di Laurea in Fisica

Facility for λ_c deuteron production in ALICE

Relatore:
Prof. Andrea Alici

Presentata da:
Giuseppe Luciano

Correlatore:
Dott. Nicolò Jacazio

Anno Accademico 2024/2025

Contents

1	Abstract	5
2	Introduction	7
3	concepts of quantum chromodynamics (QCD)	9
3.0.1	The QCD phase diagram	11
3.0.2	The different stage of a heavy-ion collision	12
4	Thermal model	17
4.0.1	hydrodynamical description	17
4.0.2	Elliptic flow	21
4.0.3	Statistical Hadronisation Model (SHM)	23
5	$Y_c N$ bound state	29
5.0.1	One Boson exchange model	29
5.0.2	Λ_c N interaction	31
5.0.3	Potential energy	35
5.0.4	Possible Λ_c supernuclei	35
6	ALICE	37
.0.1	Cooper-Frye	37

CONTENTS

Chapter 1

Abstract

Testo dell'introduzione...

Chapter 2

Introduction

Recent development of hadron spectroscopy revealed that there may exist various molecular bound states of hadrons (observed as hadron resonances) . In particular, the observation of the unexpected X, Y, and Z mesons and the follow by theoretical studies indicates that heavy quark molecules are more plausible. This can be understood from the balance between the kinetic term and the potential in the Hamiltonian: a heavier system has a smaller kinetic energy. The above naive expectation motivates us to explore possible bound states composed of is, of course, a natural extension of the hypernucleus, which is a nuclear bound state with played a key role in analysing structures of hypernuclei and extracting information on the and it is difficult to perform direct scattering experiments for the hyperons, it is important to get information on their interactions from the three-body or heavier nucleus with strange baryon(s).

There has been an impressive experimental progress in the spectroscopy of heavy hadrons, mainly in the charm sector. The theoretical analysis of hidden and open heavy flavor hadrons has revealed how interesting is the interaction of heavy hadrons, with presumably or resonances in the scattering of two hadrons with heavy flavor content. The observation of events that could be interpreted in terms of the decay of a charmed nucleus [13, 14], fostered conjectures about the possible existence of charm analogs of strange hypernuclei [15–17]. This resulted in several theoretical estimates about the binding energy and the potential-well depth of charmed hypernuclei based on one-boson exchange prospects have reinvigorated studies of the low-energy YcN interactions

Chapter 3

concepts of quantum chromodynamics (QCD)

Before talking about heavy-ion collision we can introduce some concepts of quantum chromodynamics (QCD). This theory is the most successful one to explain the strong interaction, one of the four fundamental interaction assumed in the standard model (SM), between quarks mediated by gluons. It takes its name because it introduces a property called color, the QCD analog of electric charge. Gluons are the force carriers of the theory, just as photons are for the electromagnetic force in quantum electrodynamics. First hint about the real existence of color charge was given with the discovery of Δ^{++} baryon in 1951. This baryon could be explained only imagining that it is composed of three quark u with the spin aligned observing its mass and its spin. so the configuration of the particle could be written as follows

$$|\Delta^{++}\rangle = |u_{\uparrow}u_{\uparrow}u_{\uparrow}\rangle$$

A highly symmetric configuration. However, since the particle is a fermion, it must have an overall antisymmetric wave function. In 1965, fourteen years after its discovery, this was finally understood by the introduction of colour as a new quantum number associated with the lie group SU(3). With this new parameter we can add another inner space associated to the particle and its configuration can be written

$$|\Delta^{++}\rangle = |u_{\uparrow}u_{\uparrow}u_{\uparrow}\rangle \epsilon_{ijk} [C_i \otimes C_j \otimes C_k]$$

where ϵ_{ijk} is the Ricci's tensor. Many other strong support of the assumption had been discovered with the passing of time. Quantum Chromodynamics is based on the gauge group SU(3), the Special Unitary group in 3 (complex) dimensions, whose elements are the set of unitary 3×3 matrices with determinant one. Since there are 9 linearly independent unitary complex matrices, the condition on the determinant reduced the set at 8 independent directions in this matrix space, corresponding to eight different generators of the group.

CHAPTER 3. CONCEPTS OF QUANTUM CHROMODYNAMICS (QCD)

The Lagrangian density of QCD is

$$\mathcal{L} = \bar{\psi}_q^i (i\gamma^\mu) (D_\mu)_{ij} \psi_q^j - m_q \bar{\psi}_q^i \psi_{iq} - \frac{1}{4} F_{\mu\nu}^a F^{a\mu\nu} \quad (3.1)$$

where ψ_q^j denotes a quark field with colour index, γ^μ is a Dirac matrix that expresses the vector nature of the strong interaction, with μ being a Lorentz vector index, m_q , the mass of the quark, allows for the possibility of non-zero quark masses, $F_{\mu\nu}^a$ is the gluon field strength tensor for a gluon and D_μ is the covariant derivative in QCD given by $(D_\mu)_{ij} = \delta_{ij} \partial_\mu - ig_s t_{ij}^a A_\mu^a$, with g_s the strong coupling [Skands'2013]. The QCD at low transferred momentum is not perturbative and so obtain analytical results is extremely difficult, fortunately when the transferred momentum became larger strong coupling decrease and the theory could be tested. This property has been discovered by Gross, Wilczek and Politzer and take the name of asymptotic freedom [DAVIDPOLITZER1974129].

However in typical nuclear condition the energy are too low for permit perturbative calculation but the physicist believe that a direct consequence of the theory is the confinement of hadrons, well supported by the experimental data, that exclude the possibility of find free quark. A formal proof had not been yet obtained and this problem has been added to the list of the Millennium Prize Problems. For our discussion the Polyakov loop operator gets a particular importance.

$$L = \frac{1}{3} \text{Tr} \left(P e^{ig \int_0^\beta d\tau A_4(\vec{x}, \tau)} \right) \quad (3.2)$$

Where P is the path-ordering operator and $A - 4$ is the Euclidean temporal component of the gauge field and $\beta = \frac{1}{T}$, T temperature. A vanishing thermal expectation value $\langle L \rangle$ of the Polyakov loop operator thus indicates infinite energy for a free quark, i.e. quark confinement. Studying the equation became evident that as the temperature increases $\langle L \rangle$ increases rapidly to a nonzero value at high temperatures. This indicates that quark confinement is broken at the corresponding critical temperature T_c . In the absence of quark masses the equation 3.1 is chirally symmetric. Since the up and down quark masses are very small, neglecting them is a good approximation. The nonvanishing chiral condensate at $T = 0$ breaks this chiral symmetry and generates a dynamic mass, the so called “constituent” masses. In vacuum this mass are thus about 300 MeV for the up and down quarks, about 450 MeV for the strange quark and 1.5 GeV for the charm, 4.5 GeV for bottom and 180 GeV for top. The dynamically generated mass disappeared at T_c , making the quarks light again and restoring the approximate chiral symmetry of QCD. The dissolution of massive hadrons into almost massless quarks and gluons at T_c leads to a very rapid rise of the energy density near the deconfinement transition, as shown in figure 3.1. For a massless gas of quarks and gluons the energy density is proportional to T^4 . We see that for $T \geq 4T_c$ the data remain about 20%

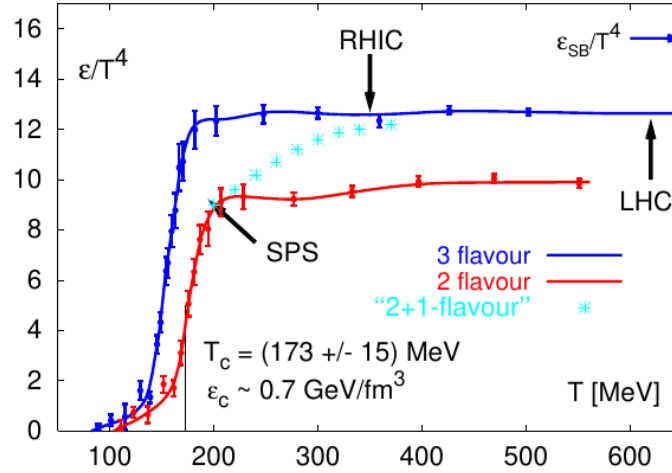


Figure 3.1: The symbol ϵ stands for energy density, the curves labelled “2 flavour” and “3 flavor” were calculated for two and three light quark flavors, “2+1 flavour” indicates a calculation for two light and one heavier strange quark flavor.

below this Stefan-Boltzmann limit. Instead near T_c the ratio ϵ/T^4 drops rapidly by more than a factor 10. This is due to hadronization. The much heavier hadrons are exponentially suppressed below T_c , leading to a much smaller number of equivalent massless degrees of freedom. The dependence of T^4 is particularly important because for exceed the critical temperature by only 30% in order to reach the upper edge of the transition region, an energy density $\epsilon \approx 3.5 \text{ GeV}/\text{fm}^3$ is required and to reach $2T_c$ the energy density needed arrived at $23 \text{ GeV}/\text{fm}^3$ [heinz2004conceptsheavyionphysics].

3.0.1 The QCD phase diagram

In QCD we have seen that the only viable option to free the hadron constituents is to increase significantly the energy scale of the system by compression or by heating. At this high energy regime hadronic matter melts releasing its elementary degrees of freedom (quark and gluons) in a way which is analogous to a phase transition. A simple description of the phases of nuclear matter is given in Fig 3.2. In order to gain insight into the dynamics of the QCD phase, many studies were performed by using lattice QCD calculations. The Quark Gluon Plasma (QGP) is hottest and most dense liquid known to humankind and according to the most widely accepted cosmological model, the Λ CDM, where the condition of our universe only few microseconds after the Big Bang. The chemical potential is a thermodynamic coordinate like the temperature, which can be best understood as the energy required by the system to change its chemical composition. It is tightly connected with the density of quarks: when the former is zero, the latter is zero as well. [QCDPhase-Diagram]. Particularly problematic is the study of the diagram when μ_B approaches 0, like in the condition of the primordial uni-

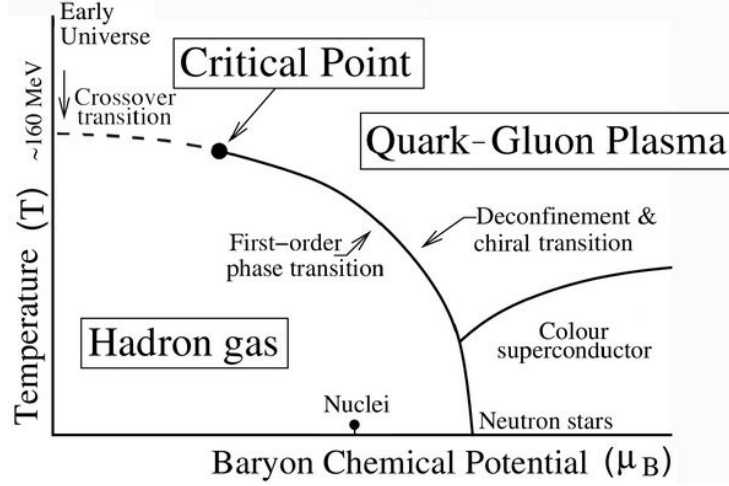


Figure 3.2: A sketched view of the phase diagram of strongly interacting matter, in the plane of temperature and the baryon chemical potential that represents the amount of net baryon charge available in the system

verse. Lattice QCD tells us that even for realistically small up and down quark masses the transition at $\mu_B = 0$ is most likely not a sharp phase transition but a rapid crossover as shown in Fig 3.2. At low temperatures and asymptotically large baryon densities quarks are also deconfined, although not in a quark-gluon plasma state but rather in a color superconductor, in these state matter carries color charge without loss, analogous to the conventional superconductors that can carry electric charge without loss. The superconducting state is separated from the QGP by a first order transition at a critical temperature estimated to be of order 30-50 MeV. Unfortunately, one cannot use heavy-ion collisions to compress nuclear matter without producing a lot of entropy and therefore also heating it; hence it seems impossible to probe with them the color superconducting phase [heinz2004conceptsheavyionphysics].

3.0.2 The different stage of a heavy-ion collision

The main stages of relativistic heavy-ion collisions are: Pre-equilibrium, thermalization, Chemical freeze-out, and decoupling. This section came mainly from [heinz2004conceptsheavyionphysics] and [amsdottorato9036].

1. Pre-equilibrium ($t \lesssim 1$ fm/c): the two nuclei just collided. The partons of every participating nucleon interact producing a large amount of quarks and gluons. The system is now formed by a dense inhomogeneous droplet of strongly interacting QGP matter. In the very early collision stages the momentum transferred is huge and the particle production can be calculated in perturbative QCD. However the strong force is the first that manifest it's effect. According to the Heisemberg uncertainty relation the production happens on a time scale $t \sim \frac{1}{\sqrt{Q^2}}$, where Q is the momentum transfers. The key difference between elementary parti-

cle and nucleus-nucleus collisions is that the quanta created in the primary collisions between the incoming nucleons can't right away escape into the surrounding vacuum, but rescatter off each other. In a central collision between two Pb or Au nuclei the nuclear reaction zone has a transverse diameter of about 12 fm, so a hard particle created near the edge and moving towards the center needs 12 fm/c before it emerges on the other side. During this time the matter thermalizes, expands, cools down and almost reaches decoupling. It does so by scattering off the evolving medium and losing energy which can be measured. The energy loss is proportional to the density of the medium times the scattering cross section between the probe and the medium constituents, integrated along the probe's trajectory. Other probes of the early collision stage are direct photons, either real or virtual, and other process connected to QED such the creation of a couple lepton-antilepton generally known as "dileptons". In contrast to all hadronic probes, they thus escape from the collision zone without reinteraction and carry pristine information about the momentum distributions of the particle that generated them. Unfortunately, the directly emitted photons and dileptons must be searched in a huge background of indirect photons and particle generated in other process, This renders the measurement of these clean electromagnetic signals difficult.

2. Thermalization ($t \sim 1 \div 10$ fm/c): the medium reaches thermal equilibrium thanks to the many interactions and the formations of new parton. The produced partons rescatter both elastically and inelastically. Both types of collisions lead to equipartitioning of the deposited energy, but only the inelastic collisions change the "chemical" composition of the medium by changing the flavor of partons. The system, now in equilibrium, builds an internal pressure that finds no opposition by the void that surrounds it. This leads to a rapid expansion of the system together with a decrease in the temperature. As the temperature lowers, the system energy density is not able to keep partons separated and hadrons start to form when the energy density approach $\epsilon \approx 1 \text{ GeV}/fm^3$. During this phase transition the entropy density drops because of the recombination. However the total entropy cannot decrease this implies that the fireball volume must increase by a large factor while the temperature remains approximately constant. Since the recombination take times the systems spend significant time near T_c .
3. Chemical freeze-out: when the temperature decreases enough inelastic interactions among hadrons have completely stopped and only the (pseudo-)elastic one occur. This happen because at this point the matter becomes so dilute that the average distance between hadrons exceeds the range of the strong interactions. The hadrons abundance "freeze out" but the creation of some resonance is however possible but such pro-

CHAPTER 3. CONCEPTS OF QUANTUM CHROMODYNAMICS (QCD)

cesses don't change the finally observed chemical composition. Since most of the hadrons in a relativistic fireball are pions, very light particle $m_\pi \sim 140$ MeV, resonances with them are very efficient in keeping the system in thermal equilibrium.

4. Kinetic freeze-out: at this stage the hadrons, including the then present unstable resonances, start to decouple from the medium as the temperature lowers and the mean free path becomes larger than the mean distance between hadrons. This results in a complete stop of all interactions. Now the repartition of the kinetic energy among all hadrons has stopped and the transverse momentum spectrum is approximately exponential. The unstable resonances decay in particle with smaller transverse momenta. Since most resonances decay by emitting a pion, this effect is particularly important for the pion spectrum which at low p_\perp are completely dominated by decay products.

A graphical resume of the process is visible in Fig 3.3 and 3.4

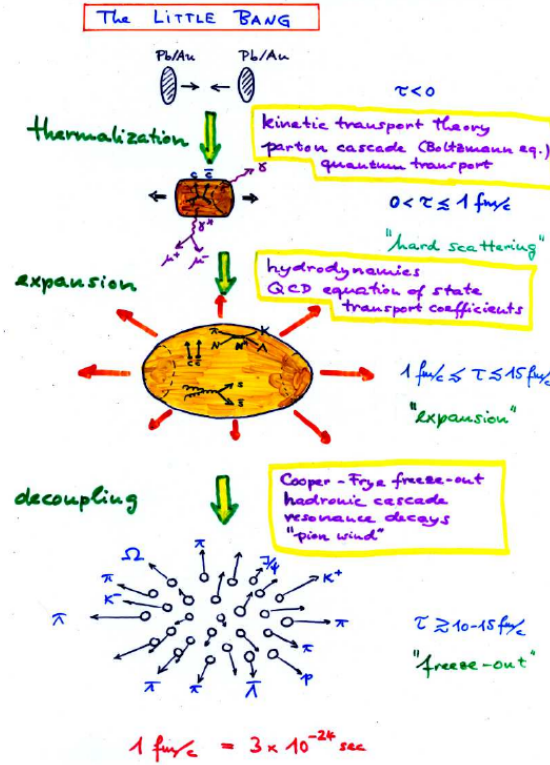


Figure 3.3: A sketched view of the phase of the system after the collision

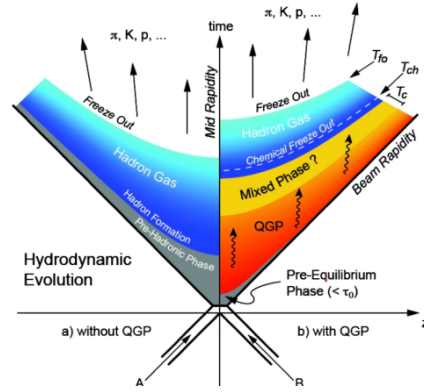


Figure 3.4: Evolution of a central heavy ion collision in a Minkowski-like plane. The two scenarios with and without QGP are pointed out. The critical temperature is indicated by T_c , while the freeze-out and chemical freeze-out temperatures, are pointed out with T_{fo} , and T_{ch} , respectively [EvolutionofcollisionsandQGP].

CHAPTER 3. CONCEPTS OF QUANTUM CHROMODYNAMICS (QCD)

Chapter 4

Thermal model

4.0.1 hydrodynamical description

This section resume the information of [heinz2004conceptsheavyionphysics], [phdthesis], [Cooper-Frye].

The fireball can be approximately described as an ideal fluid if the microscopic scattering time scale is much shorter than any macroscopic time scale associated with the fireball evolution. Hydrodynamics becomes applicable when the mean free path of the particles is much smaller than the system size, and allows for a description of the system in terms of macroscopic quantities. The hydrodynamic equations require knowledge of the equation of state that in this case must connect the pressure, the energy density and baryon density. Hydrodynamics is the ideal language for relating observed collective flow phenomena because it allows ad description of the hadronization phase transition without any need for a microscopic description.

For define the collective flow we can consider any space-time point in the fireball and considered an infinitesimal volume associate with the point. So the flow velocity can be expressed by $\vec{v}(x) = \frac{\vec{P}}{P^0}$, where \vec{P} is the mean 3-momentum of the particle in the volume and P^0 is the mean energy in quadrivectorial formalism. With $\vec{v}(x)$ we can associate a normalized velocity $u^\mu = \gamma(\vec{v}(x) = \frac{1}{\sqrt{1-v(x)^2}})$ In the same manner it's we define $T(x)$ the average local temperature and the μ_i , the chemical potential of the i-th particle species. It's possible to separate the flow velocity into its components along the beam direction ("longitudinal flow" $\vec{v}_l(x)$) and in the plane perpendicular to the beam ("transverse flow" $\vec{v}_\perp(x)$). From now on we use the unit $c=1$, $\hbar=1$. In this case the phase-space distribution of particles of type i is given by the Lorentz covariant local equilibrium distribution

$$f_{i,eq}(x, p) = \frac{g_i}{e^{(p \cdot u - \mu_i)/T} \pm 1} = g_i \sum_{n=1}^{\infty} (\pm)^n e^{n(p \cdot u - \mu_i)/T} \quad (4.1)$$

Here g_i is a spin-isospin-color-flavor-etc. degeneracy factor which counts all particles with the same properties. The factor $p \cdot u$ is the energy of the

particle in the local rest frame. The ± 1 in the denominator accounts for the proper quantum statistics of particle (-1 for fermions and +1 for boson). The Boltzmann approximation corresponds to keeping only the first term in the sum over n in the last expression. In our applications this is an excellent analytical approximation for all hadrons except for the pion because of their mass.

At relativistic energies it is convenient to parametrize the longitudinal flow velocities and momenta in terms of rapidities, $\eta = \frac{1}{2} \ln \frac{1+v}{1-v}$ in this way $v = \tanh \eta$. It's also possible to define $\eta_l = \frac{1}{2} \ln \frac{1+v_l}{1-v_l}$ and $y = \frac{1}{2} \ln \frac{1+\frac{p_l}{E}}{1-\frac{p_l}{E}} = \frac{1}{2} \ln \frac{E+p_l}{E-p_l}$. Bjorken argued that at asymptotically high energies the physics of secondary particle production should be independent of the longitudinal reference frame. Furthermore, the boost-invariance of these initial conditions is preserved in longitudinal proper time if the system expands collectively along the longitudinal direction, in this approximation hold $\eta = \eta_l$. For more detail see [PhysRevD.27.140]. The Bjorken scaling approximation is expected to be good at high energies and not too close to the beam and target rapidities, i.e. in safe distance from the longitudinal kinematic limits. With Bjorken intuition.

$$p \cdot u(x) = \gamma_{\perp}(\vec{r}_{perp}, \tau) (m_{perp} \cosh(y - \eta) - \vec{p}_{\perp} \cdot \vec{v}_{perp}(\vec{r}_{perp}, \tau)) \quad (4.2)$$

Where $\vec{r}_{perp} = (x, y)$, $m_{\perp} = \sqrt{m^2 + p_{\perp}^2}$ is the transverse mass, $\tau = \sqrt{t^2 - z^2}$ is the longitudinal proper time and z the longitudinal position.

The Cooper-Frye formula

Suppose we want to count the total number of particles of species i after produced in the collision. Since this number does not depend on the reference frame of the observer, we must be able to express it in a Lorentz-invariant way. We define a three-dimensional hypersurface $\Sigma(x)$ in 4-dimensional space-time along which we perform the counting. Different choices for the 3-dimensional hypersurface Σ are possible as long as it completely closes off the future light cone emerging from the collision point. We count particles crossing the surface by subdividing it into infinitesimal elements $d^3\sigma$, defining an outward-pointing 4-vector $d^3\sigma_{\mu}(x)$ perpendicular to $\Sigma(x)$ at point x with the magnitude $d^3\sigma$. Introducing the 4-vector j_i^{μ} describing the current of particles i through point x , and summing over all the infinitesimal hypersurface elements we get

$$N_i = \int_{\Sigma} d^3\sigma_{\mu}(x) j_i^{\mu}(x) = \int_{\Sigma} d^3\sigma_{\mu}(x) \left(\frac{1}{(2\pi)^3} \int \frac{d^3p}{E} p^{\mu} f_i(x, p) \right) \quad (4.3)$$

Where $j_i^{\mu}(x)$ is given in terms of the Lorentz-invariant phase-space distribution (giving the probability of finding a particle with momentum p at point x) by

multiplying it with the velocity $\frac{p^\mu}{E}$ and integrating over all momenta with measure $\frac{d^3p}{(2h\pi)^3} = \frac{d^3p}{(2\pi)^3}$. We finally obtain the Cooper-Frye formula

$$E \frac{dN_i}{d^3p} = \frac{dN_i}{dy p_\perp dp_\perp d\phi_p} = \frac{dN_i}{dy m_\perp dm_\perp d\phi_p} = \frac{1}{(2\pi)^3} \int_\Sigma p \cdot d^3\sigma_\mu(x) f_i(x, p) \quad (4.4)$$

with ϕ_p is the azimuthal angle. To compute the measured momentum spectrum we can therefore replace the surface Σ corresponding to the detector by shrinking it to the smallest and earliest surface that still encloses all scattering processes. We call this the “surface of last scattering” or “freeze-out surface” Σ_f . The the number of particles obtained from the Cooper-Frye formula is not always positive-definite. Physically negative contributions of the Cooper-Frye formula are particles that stream backwards into the hydrodynamical region. It’s possible to compare the negative contribution with the total number particles crossing the transition hypersurface. It is found that the number of underlying inward crossings is much smaller than the one the Cooper-Frye formula gives under the assumption of equilibrium distribution functions.

to compute the measured momentum spectrum requires knowledge of the phase-space distribution on the surface of last scattering. If the system expands very fast, its density decreases rapidly and the mean free path of the particles growth quickly. The transition from strong coupling to free-steaming thus happens in a short time interval. During this short time it is unlikely that the phase-space distribution undergoes qualitative changes, and we may approximate $f_i(x, p)$ on the last scattering surface by its thermal equilibrium form that it still had just a little earlier. In this section we report only the final result but the proof could be find in the appendix.

$$\frac{dN_i}{dy m_\perp dm_\perp d\phi_p} = \frac{g_i}{\pi} \int_0^\infty r_\perp dr_\perp n_i(r_\perp) \left[m_\perp K_1 \left(\frac{m_\perp \cosh(\rho(r_\perp))}{T(r_\perp)} \right) I_0 \left(\frac{p_\perp \sinh(\rho(r_\perp))}{T(r_\perp)} \right) - p_\perp \frac{\partial \tau}{\partial r_\perp} \right] \quad (4.5)$$

Where appear the modified Bessel functions and $v_\perp = \tanh \rho$. This formula is useful because it allows to easily perform systematic studies of the influence of the radial profiles of temperature, density and transverse flow on the transverse momentum spectrum, in order to better understand which features of a real dynamical calculation of these profiles control the shape of the observed spectra.

Transverse momentum spectra and freeze-out temperature

For all hadrons is observed that $m_\perp/T > 1$ so the modified Bessel function can be approximate in the following manner $K_\nu \sim e^{-\frac{m_\perp \cosh \rho}{T}}$. Since temperature on the freeze-out hypersurface is approximately constant and that the freeze-out volume is controlled by the mean free path which is inversely proportional to the density, which itself is a steep function of temperature. At $r_\perp = 0$ the radial flow velocity must vanish by symmetry but to larger

r_\perp typically rises linearly. , it eventually reaches a maximum value and drops again to zero since the dilute tail of the initial density distribution freezes out early. Some simulated profile of grow are shown in the Fig 4.1 [teaney2001hydrodynamicdescriptionheavyion].

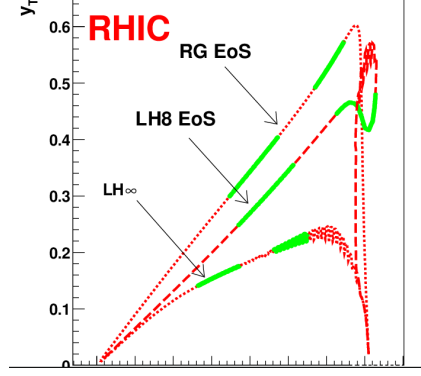


Figure 4.1: Radial flow rapidity profile $\rho(r_\perp) = y_T$ for central Au+Au collisions at RHIC, from hydrodynamic calculations employing three different equations of state [EvolutionofcollisionsandQGP].

Different process can manifest, for example at SPS energies the freeze-out surface moves from the edge inward since the fireball matter cools and freezes out faster than the developing radial flow can push it out. At LHC energies the much stronger radial flow generated by the much higher internal pressure makes the fireball grow considerably before suddenly freezing out after about 13 fm/c. For understand how the radial flow influence the spectra first consider the absence of flow ($\rho = 0$), in this condition $I_q(0) = 0$ so the equation 4.5 reduced to

$$\frac{dN_i}{dm_\perp dm_\perp} \sim m_\perp K_1\left(\frac{m_\perp}{T}\right) \sim m_\perp^{1/2} e^{-\frac{m_\perp}{T}} \quad (4.6)$$

In these condition as the temperature is the same for all hadron the spectra depend only on the transverse mass, a fact known as " m_\perp " scaling. As visible in the equation the temperature can be extracted easily. Instead if the radial flow is not vanishing approximating $p_\perp \approx m_\perp$ one get.

$$\frac{dN_i}{dm_\perp dm_\perp} \sim e^{-\frac{m_\perp (\cosh \rho - \sinh \rho)}{T}} = e^{-\frac{m_\perp}{T_{slope}}} \quad (4.7)$$

With $T_{slope} = T \sqrt{\frac{1+v_\perp}{1-v_\perp}}$ It is most extreme for a thin shell expanding with fixed velocity ("blast wave"), shown in Fig 4.2, in which case for sufficiently large hadron mass and flow velocity the spectrum develops a blast wave peak at nonzero transverse momentum. In conclusion is possible to summarize these two important limits

$$\text{Non relativistic: } p_\perp \ll m_i \quad T_{i,slope} \approx T_f + \frac{1}{2} m_i \langle v_\perp \rangle^2 \quad (4.8)$$

$$\text{Relativistic: } p_{\perp} \gg m_i \quad T_{\text{slope}} = T \sqrt{\frac{1+v_{\perp}}{1-v_{\perp}}} \quad (4.9)$$

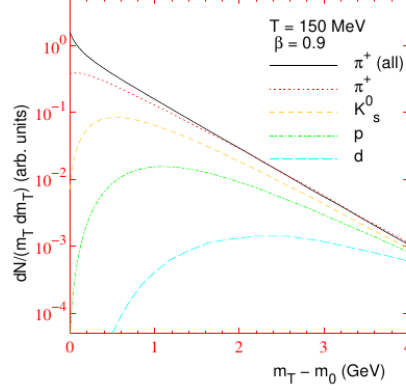


Figure 4.2: Flow spectra for various hadrons as a function of $m_{\perp} - m_0$ where m_0 is their rest mass. The calculation assumes an infinitesimally thin shell of temperature $T = 150$ MeV expanding with $v_{\perp} = 0.9$. The curve labelled " π^+ (all)" includes pions from resonance decays in addition to the thermally emitted pions.

4.0.2 Elliptic flow

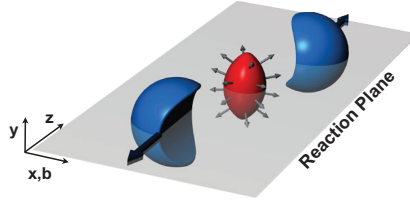


Figure 4.3: Almond shaped interaction volume after a non-central collision of two nuclei. The spatial anisotropy with respect to the x-z plane (reaction plane) translates into a momentum anisotropy of the produced particles (anisotropic flow).

this section come from [Snellings'2011], [heinz2004conceptsheavyionphysics] [Kolb'2000]. For central collisions between equal spherical nuclei, radial flow is the only possible type of transverse flow allowed by symmetry. In non-central collisions between this azimuthal symmetry is broken and anisotropic transverse flow patterns can develop. The overlap region of the two colliding nuclei is then spatially deformed in the transverse plane. Experimentally, the most direct evidence of flow comes from the observation of anisotropic flow which is the anisotropy in particle momentum distributions correlated with the reaction plane. The evolution of the almond shaped interaction volume is shown in Fig 4.4 [kolb2003hydrodynamicdescriptionultrarelativisticheavyion]. The contours indicate the energy density profile and the sequence show the time evolution from an almond shaped transverse overlap region into an almost symmetric system. This expansion happen at the speed of speed velocity $v_s = \sqrt{\frac{\partial p}{\partial \epsilon}}$. In this situation the equation 4.4 can be written using a Fourier

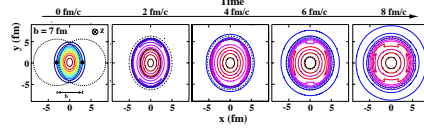


Figure 4.4: The created initial transverse energy density profile and its time dependence in coordinate space for a non-central heavy-ion collision. The z-axis is along the colliding beams, the x-axis is defined by the impact parameter.

expansion and introducing b , the impact parameter, in the form

$$E \frac{dN_i}{d^3p}(b) = \frac{dN_i}{dy p_\perp dp_\perp d\phi_p}(b) = \frac{1}{2\pi} \frac{dN_i}{dy p_\perp dp_\perp}(b) \left(1 + 2 \sum_{n=1}^{\infty} v_2^n(p_\perp, b) \cos(n\phi_p) \right) \quad (4.10)$$

In this Fourier decomposition, the coefficients v^1 and v^2 are known as directed and elliptic flow, respectively. The overlap region of the two colliding nuclei is then spatially deformed in the transverse, as visible in Fig 4.3, plane so the momentum space distribution changes in the opposite direction from being approximately azimuthally symmetric to having a preferred direction in the reaction plane. The asymmetry in momentum space can be quantified by the spatial ellipticity:

$$\epsilon_x(b) = \frac{\langle y^2 - x^2 \rangle}{\langle y^2 + x^2 \rangle} \quad (4.11)$$

As a function of time ϵ_x decreases, spontaneously due to free-streaming radial expansion (if no rescattering happens) or somewhat more quickly due to the development of elliptic flow (if rescattering occurs) which makes the system expand faster into the reaction plane than perpendicular to it. The first mechanism is a consequence of the Heisenberg uncertainty principle because if the definition in the position is higher the uncertainty on the linear momentum in the same direction is higher and the particle can move faster. Instead the elliptic flow is a consequence of the fact that there is high pressure in the interior of the reaction zone which falls off to zero outside. the pressure gradient is so steeper in the short direction, leading to stronger hydrodynamic acceleration. Hydrodynamics predicts that heavier particles gain more momentum than lighter ones, leading to the previously discussed flattening of their spectra at low transverse kinetic energies. It's possible to show that the spatial eccentricity decrease as a function of time in the following manner, the proof is in the appendix.

$$\frac{\epsilon_x(\tau_0 + \Delta\tau)}{\epsilon_x(\tau_0)} = \left[1 + \frac{(c\Delta\tau)^2}{\langle \vec{r}^2 \rangle_{\tau_0}} \right]^{-1} \quad (4.12)$$

where τ_0 is the time when the particles were created and $\langle \vec{r}^2 \rangle_{\tau_0}$ is the azimuthally averaged initial transverse radius squared of the reaction zone. So if thermalization is delayed by a time $\Delta\tau$, any elliptic flow would have to build on a reduced spatial deformation and would come out smaller. It is also

known from microscopic kinetic studies that for a given initial spatial eccentricity the magnitude of the generated elliptic flow is a monotonic function of the mean free path that can be rewritten by the product of density and scattering cross section in the fireball.

More recently, it was realized that small deviations from ideal hydrodynamics, in particular viscous corrections, already modify significantly the buildup of the elliptic flow. The shear viscosity determines how good a fluid is, however, for relativistic fluids the more useful quantity is the shear viscosity over entropy ratio η_v/s . For perfect fluids the ratio can be approximated by:

$$\frac{\eta_v}{s} \approx \frac{\hbar}{4\pi k_B} \quad (4.13)$$

It is argued that the transition from hadrons to quarks and gluons occurs in the vicinity of the minimum in η_v/s , just as is the case for the phase transitions in helium, nitrogen, and water. The fact that the QGP behaves like an ideal fluid implies strong non-perturbative interactions in the quark-gluon plasma phase.

4.0.3 Statistical Hadronisation Model (SHM)

this section had been inspired by the following article [[becattini2009introductionstatisticalhad](#) [[charm`hierarchy`in`the`statistical`hadronization`model](#)] [[heinz2004conceptsheavyionp](#)

The idea of applying statistical concepts to the problem of multi-particle production in high energy collisions dates back to a work of Fermi in 1950, who assumed that particles originated from an excited region evenly occupying all available phase space states. The microscopic description of the process in which thousand of quarks and gluons combine to form thousands of final state hadrons is an impractical problem. Note that such a statistical approach has, of course, its limitations. In fact investigating correlations between pairs, triplets, quadruplets etc. of particles, because they all belong to a single collision and are not produced entirely independently. For example the momenta of thousand of particle emerging from the fireball must conserve the original momentum of the initially colliding nuclei probably generating non-statistical momentum correlations among considerably smaller subclusters of particles. So for describe this complex dynamical process, the Statistical Hadronisation Model (SHM) postulates that hadrons are formed from the decay of each cluster in a purely statistical way so.

Every multihadronic state localized within the cluster and compatible with conservation laws is

The volume of the system created in heavy-ion collisions is considerably larger than the partonic scale, this justifies the usage of a grand-canonical ensemble. Under these conditions the elementary volume under study can exchange both particles and energy with its surroundings meaning that the quantum numbers are conserved. In particular the volume of clusters is in a constant ratio with their mass when hadronization takes place. In addition

one has to consider the quantum behaviour of both fermionic and bosonic degrees of freedom that form the system. Quantum interference effects in the production of identical particles, the so-called Bose-Einstein correlations or Hanbury Brown-Twiss second-order interference would simply be impossible without a finite volume. The Bose-Einstein correlations (BEC) refer to a quantum mechanical phenomenon that arises due to the wave-like nature of bosonic particles and their tendency to occupy the same quantum state. Instead the Hanbury Brown and Twiss (HBT) effect is any of a variety of correlation and anti-correlation effects in the intensities received by two detectors from a beam of particles. HBT effects can generally be attributed to the wave-particle duality of the beam, and the results of a given experiment depend on whether the beam is composed of fermions or bosons. From statistical mechanics is known that hold

$$\langle N \rangle = \frac{1}{\beta} \left(\frac{\partial \ln Z}{\partial \mu_B} \right) \langle E \rangle = - \left(\frac{\partial \ln Z}{\partial \beta} \right) + \mu_B \langle N \rangle \langle S \rangle = k_B \frac{\partial T \cdot \ln Z}{\partial T} P_{pressure} = \frac{1}{\beta} \left(\frac{\partial \ln Z}{\partial V} \right) \quad (4.18)$$

for a given species i can be split into each conserved quantify: $i = B_i B + S_i S + Q_i Q$, where B_i , S_i and Q_i are respectively the baryon number, strangeness and electric charge while B , S and Q are the corresponding chemical potentials. For smaller systems ($e+e$, pp and p - Pb) the grand-canonical ensemble is no longer a good description of the system. In this case the volume created after the collision is considerably smaller and it is better to require the local conservation of quantum numbers (at least for the strangeness quantum number) and allow only energy exchanges among volumes (canonical formulation). A detailed description of the partition function for the canonical ensemble can be found in [36]. Nonetheless the grand-canonical approach is commonly used to treat central heavy-ion collisions where the system created has large spacial extension. Different statistical hadronization (thermal) models (SHM) implement the basic formula in Eq. 2.6 [36–38]. These models differ from each other in the number of free parameters, the corrections applied and on the type of ensemble used. Some include a hadronic phase with residual chemical activity based on the Ultra-Relativistic Quantum Mechanics Dynamics model (UrQMD)1. Other models make use of a flavor-dependent chemical decoupling by introducing s as the strangeness suppression factor. In this case s takes into account the possibility to have partial thermalization for strange quarks, as it will be explained later, it is expected to have $s \leq 1$ in small collision systems (where the canonical ensemble i.e. local conservation of quantum number is imposed) while in heavy-ion collisions the s quarks can be fully thermalized and s can reach values of 1. The common aim among all these models is to predict global properties of the medium by using the “soft probes” (or light flavor) which are thermal produced. These observables have the advantage of being commonly produced in each collisions and form a basic measurement for every experimental setup. Starting from measurements of

the identified particle yields (dN/dy) in the light flavor sector by using the SHM approach one gains the access to the thermodynamic properties of the system created in the collision. In principle the more particle species are measured the better, in fact all particle that are produced at equilibrium can be used for this purpose. An example of such measurement for different particle species (\pm , K^\pm , p , \bar{p} , and Λ) is given in Fig. 2.1 as a function of the $\sqrt{s_{NN}}$ for central collisions. At first glance it is possible to see the large evolution in particle production and identify some key features:

1. All particles and their corresponding anti-particles tend to be equally produced if the collision energy is high enough. This is especially true at LHC energies [39, 40].
2. Baryons (p and \bar{p}) and mesons (K and \bar{K}) follow different behaviour with significant baryon/anti-baryon discrepancies at lower energies.
 - The yields of p lowers while \bar{p} increase with $\sqrt{s_{NN}}$, in relation to the decrease of B . When B is larger than 0 the baryonic number of the colliding nuclei is to be found in the products of the collision. At low energies, an important fraction of the initial colliding nucleons are found in the final state (large stopping power). For larger beam energies the colliding nuclei become almost transparent to each other (no baryon stopping). At this energy regime the products of the primordial nucleons are less likely to be found in the final states.
 - The production of Λ , similar to p , is affected by the non-zero B at low energies but the effect is reduced since it contains an s quark. At intermediate energies exhibits a decrease similar to that of p .
3. At high energies, pions are the most abundant particle species produced
4. Particles containing s quarks are subject to a significant increase in their abundances above the SPS energies. This effect known as “strangeness enhancement” was historically identified as a signature typical of the QGP. This topic will be the subject of Section 2.1.1.
5. At high energies the production of particles with same mass but different quark content tends to be similar (e.g. p and \bar{p}). The SHM can be used to fit the measured dN/dy to fix its parameters. This is done by using only a limited number of parameters (T , V , s , B) and carrying out the calculation with the best ensemble for the collision system. This allows to obtain quantities such as the chemical freeze-out temperature T_{Ch} , the system volume V and the chemical potential B . Results from [41] (Fig. 2.2) show how the best fit parameters to describe the data from Pb–Pb central collisions collected by the ALICE experiment at $\sqrt{s_{NN}} = 2.76$ TeV are: $T = 156.5 \pm 1.5$ MeV, $B = 0.7 \pm 3.8$ MeV, $V = 5280 \pm 410$ fm³. The model is able to describe reasonably well measurements of yields which span over 9 order of magnitudes with a $\chi^2/NDF = 1.61$ with a low number of free parameters. The largest tension is observed for p and \bar{p} , reaching almost a 3 deviation. The effectiveness of the thermal model predictions is not only limited to the high energy of the LHC but covers lower collision energies as shown in Fig. 2.3. In this case both K/π and p/π are well reproduced by the model over a wide range of energies. The advantage of comparing the model to yield ratios instead of simple yields lays in cancelling out the dependence

on the source volume V (Eq. 2.6). to the one sketched in Fig. 1.3. In addition these results allow for a direct comparison with predictions from lattice QCD. The T_{Ch} temperature obtained from thermal model fits can be compared with the predictions for the critical temperature of the phase transition T_c obtained from lattice QCD calculations at vanishing B [41]. Such comparison is shown in Fig. 2.4a. It is worth to note that the chemical decoupling happens at T_{Ch} which is fully consistent with the values of T_c (154 ± 9 MeV [19]) predicted by lattice QCD. This indicates that the hadronization occurs few instants before the chemical freeze-out. The SHM is not only limited to heavy-ion collisions at it can also be applied to small systems such as pp and e+ e collisions. In this case [49] it is necessary to perform the computations in the canonical ensemble (at least requiring local strangeness conservation).

If the hadronization process does not change the number of ss pairs (for example, because strange valence quarks are too heavy), we should implement an additional constraint on the total number of strange quarks and antiquarks which fixes that number to the value before hadronization begins. In this case the expression for i in (85) generalizes to $i = B_i B + S_i S + \dots$ where S_i is the total number of strange quarks and antiquarks in hadron i and s is a further Lagrange multiplier related to this additional constraint. The associated fugacity $s = e^s$ is known as the “strangeness saturation factor” [142]. An under- resp. oversaturation of the strange particle phase space relative to its chemical equilibrium value corresponds to $s < 1$ resp. $s > 1$. Equation (85) is a local thermal and chemical equilibrium distribution function. If the system could be kept at constant volume, any type of strong interaction among the hadrons would leave this distribution unchanged since such microscopic processes again conserve energy, baryon number and strangeness. However, the apparent “equilibrium” expressed by Eq. (85) is not achieved kinetically (i.e. as a result of hadronic rescattering) but statistically (by interference of many different hadron production channels). It is very important to realize that the same local equilibrium distribution (85) can be the result of two conceptually entirely different types of processes: we can either take system of hadrons with an arbitrary (except for the constraint on total energy, baryon number and strangeness) initial phase-space distribution and let it evolve for a sufficiently long time to obtain Eq. (85) as a result of the action of elastic and inelastic processes among the hadrons. This is kinetic equilibration. Or we produce the system of hadrons of given energy, baryon number and strangeness from some non-hadronic state by a statistical process which fills hadronic phase-space in the statistically most probable configuration. This is statistical equilibrium. Both processes share the property that they lead to a state of Maximum Entropy. However, statistical hadronization can produce a Maximum Entropy distribution through non-hadronic processes which occur much faster than any inelastic scattering among hadrons at the given energy and baryon number density. you try to create, via statistical hadronization, a “pre-established equilibrium” distribution (85) of hadrons at energy density

e \leq e_{cr} ($T \leq T_{cr}$), lattice QCD tells us that such a “superheated” hadronic equilibrium configuration is unstable against deconfinement. If you leave this system to itself, the hadrons will dissolve again into quarks and gluons. Statistical hadronization thus can only proceed once the energy density has dropped to $e_{had} = e_{cr} \approx 1 \text{ GeV/fm}^3$. Therefore the hadrons, when first formed from the hadronizing quark-gluon state, will have apparent chemical equilibrium abundances corresponding to a temperature $T_{had} = T_{cr}$.⁴ Before discussing what happens to this “chemical temperature” after hadronization has been completed, let us first have look at the data.

envisaged: either hadronizing clusters are simply much larger than those in elementary collisions; or clusters are hydrodynamical cells, i.e. they are small but in thermal contact with each other due to previous thermalization, which implies a strong correlation between their position and momentum and charge densities (see Fig. 7). In both case the canonical or grand-canonical formalisms apply to individual clusters. For the former case, it is worth mentioning that the transition from a canonical to a grand-canonical description effectively occurs when the cluster volume is of the order of 100 fm^3 at an energy density of 0.5 GeV/fm^3 .

In the framework of the hydrodynamical model, formula (26) applies to individual clusters identified with hydrodynamic cells and both temperature and chemical potentials depend on space-time; when integrating particle densities to get average multiplicities, one should take into account this dependence. It is important to stress that the hydrodynamical description is a salient feature of heavy ion collisions due to the early thermalization of the system in the partonic phase, a phenomenon which does not occur in elementary collisions. It is this early thermalization which establishes the strong correlation between positions and velocities of clusters, supposedly absent in elementary collisions. Provided that rapidity distributions are wide enough, and that there is little variation of the thermodynamical parameters of clusters around midrapidity, the formula (26) describes rapidity densities of hadrons at midrapidity as well: this condition is fulfilled at RHIC energies, but not at AGS and SPS energies, where the measured rapidity distributions are not significantly wider than those of a single fireball at the temperature found [22]. In general, the fits to particle multiplicities in heavy ion collisions are of the same good quality as in elementary collisions (see Fig. 8). Many groups have analyzed the data over more than a decade [3] and the overall description is very good throughout all explored energies and one finds a smooth curve in the $T - B$ plane (see Fig. 9).

Chapter 5

$Y_c N$ bound state

5.0.1 One Boson exchange model

Before the publications of Hideki Yukawa's papers in 1935 [yukawa] physicists cannot explain the results of James Chadwick's atomic model, which consisted of positively charged protons and neutrons packed inside of a small nucleus, with a radius on the order of $10^{-14} - 10^{-15}$ m. This because the electromagnetic forces at these lengths would cause these protons to repel each other and for the nucleus to fall apart. For these reason in 1932, Werner Heisenberg proposed a "Platzwechsel" (migration) interaction between the neutrons and protons inside the nucleus, in which neutrons were composite particles of protons and electrons. These composite neutrons would emit electrons, creating an attractive force with the protons, and then turn into protons themselves [heisemerg]. The model just explained violate the linear and anglular momentum and for these reason Enrico Fermi in 1934 proposed the proposed the emission and absorption of two light particles: the neutrino and electron, rather than just the electron. Some month later the soviet physicists Igor Tamm and Dmitri Ivanenko demonstrated that the force associated with the neutrino and electron emission was not strong enough to bind the protons and neutrons in the nucleus.

For these reasons Hideki Yukawa combines both the idea of Heisenberg's short-range force interaction and Fermi's idea of an exchange particle in order to fix the issue of the neutron-proton interaction. For introducing the Yukawa's potential we can start from the Klein-Gordon equation that governs dynamics of free massive scalar, without spin, field

$$\nabla^2 \phi(\vec{r}, t) - \frac{1}{c^2} \frac{\partial^2 \phi(\vec{r}, t)}{\partial^2 t} = \frac{m^2 c^2}{\hbar^2} \phi(\vec{r}, t) \quad (5.1)$$

where ϕ is the wave function, \vec{r} the position, t the time, and m the mass of the particle. In spherical coordinate becomes for the radial component.

$$\frac{1}{r^2} \frac{\partial}{\partial r} (r^2 \frac{\partial}{\partial r} \phi(\vec{r}, t)) - \frac{1}{c^2} \frac{\partial^2 \phi(\vec{r}, t)}{\partial^2 t} = \frac{m^2 c^2}{\hbar^2} \phi(\vec{r}, t) \quad (5.2)$$

A solution for the second equation is.

$$\phi(\vec{r}, t) = -g^2 \hbar c \frac{e^{\frac{i}{\hbar}(\vec{r} \cdot \vec{P} - Et)}}{r} \quad (5.3)$$

Where \vec{P} is the linear momentum and E the energy. For virtual particles hold that $0 \sim p^2 c^2 + m^2 c^4$ so $p \sim \pm i m c$ and with the Einstein-De Broglie equation one get that $\lambda = \frac{\pm i \hbar}{m c}$, named Compton wave length, and the solution can be rewritten as

$$\phi(\vec{r}, t) = -g^2 \hbar c \frac{e^{-\frac{r}{\lambda}}}{r} = -g^2 \hbar c \frac{e^{-\frac{r m c}{\hbar}}}{r} \quad (5.4)$$

after have rejectes the divergent solution. The equation 5.4 clarify that massive mediators gives short range interaction. A graphical representation of the phenomena is visible in the pictures, 5.1. Yukawa used his equation aslo to

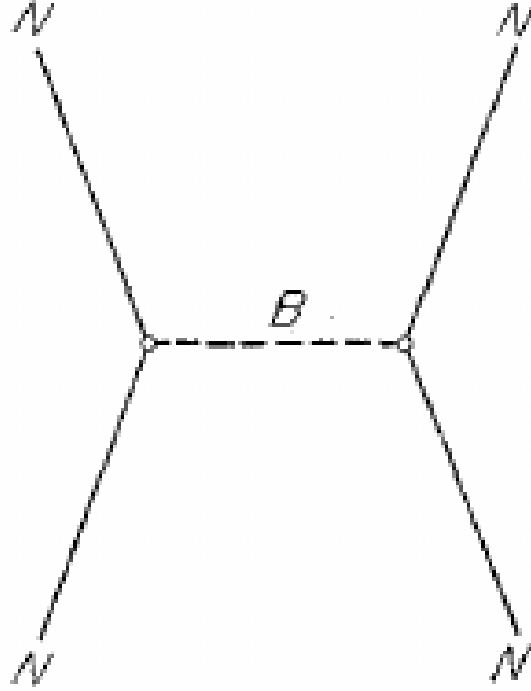


Figure 5.1: The one-boson-exchange diagram of the nucleon-nucleon scattering.

predict the mass of the mediating particle as about 200 times the mass of the electron ~ 140 Mev. Physicists called this particle the "meson," as its mass was in the middle of the leptons and barions. Yukawa's meson was found in 1947, and came to be known as the pion. The model has been referred

to as the "one-boson-exchange model" (OBE model) or the "one-particle-exchange model". This model has presented a new possibility for the realistic understanding of nuclear forces. Basing on the Yukawa potential the Sakata [sakata] model was created with the aim of giving a systematic understanding not only of the nucleon-nucleon interaction but of other various strong reactions. In this model, mesons and baryons are considered as composite systems of the fundamental particles: proton (p), neutron (n) and λ -particle (λ), and their antiparticles. With other generalization these works predicted the existence of many resonance levels including the octet mesons now established and seemed to support the basic features of the Sakata model and it became clear from experiment that the wide-spread existence of these resonance levels is one of the fundamental features of the baryon-meson system. From analysis of pion production processes, etc., by the isobar model in which the resonance states are regarded as particles was noted that: The treatment of a resonance as an "elementary" particle has considerable applicability and the non-correlated final states play only a minor role. For these reason the strong interactions should be derived from the fundamental interactions between the fundamental particles, and the Yukawa interaction observed between pion and nucleon is regarded as an effective Hamiltonian which results from the fundamental interactions including all the higher order corrections on the system of composite particles. Higher order effect should not be taken for the Yukawa interaction as because such effects should be considered in the fundamental interaction, not for the model Hamiltonian. Furthermore The Yukawa interaction, as a model Hamiltonian, already contain some of the higher order effects of the fundamental interaction in a certain correlated form. In conclusion we cannot logically exclude the possibility that there may remain some higher order effects of the fundamental interactions not represented by the lowest order diagram and that the higher order of the model interaction might represent such parts. However, we are interested in the OBE model as a zeroth order trial. [onebosonexchangepotentialmodelapproach].

5.0.2 Λ_c N interaction

This section is a resume of the [Charmed-nucleon] and [baryonnucleon-potential] Constructing a model for describe with first-principles analytical calculations of non-perturbative quantum chromo-dynamics (QCD) phenomena is very limited. Furthermore the lack of experimental information on the elementary Y_c N makes the describing of the formation of bound states much more difficult. Thus, the situation can be ameliorated with the use of well constrained models based as much as possible on symmetry principles and analogies with other similar processes, which is still a valid alternative for making progress.

A model was proposed in the early 1990s in an attempt to obtain a simultaneous description of the light baryon spectrum and the nucleon-nucleon interaction [Valcarce'2005]. It was later on generalized to all flavor. In this

model, hadrons are described as clusters of three interacting massive (constituent) quarks. The masses of the quarks are generated by the dynamical breaking of the original $SU(2)_L \otimes SU(2)_R$ chiral symmetry of the QCD Lagrangian at a momentum scale of the order of $\Lambda_{\text{QCD}} = 4\pi f_\pi \sim 1$ GeV, where f_π is the pion electroweak decay constant.

In fact massless fermions in Dirac theory are described left or right-handed spinors that each have 2 complex components. These have spin either aligned (right-handed chirality), or counter-aligned (left-handed chirality), with their momenta. In this case chirality is a conserved quantum number of the fermion and the description of the can be spinous can be reduced in these space. A Dirac mass term explicitly breaks the symmetry but in QCD, the lowest mass quarks are nearly massless and exist an approximate chiral symmetry. The vacuum in QCD is non-trivial. It does not simply consist of empty space; rather, it has a rich structure in which quark-antiquark pairs are continually being created and annihilated. This is sometimes referred to as the QCD vacuum. This vacuum is described as a superposition of many states, and the interactions between quarks and gluons cause the system to prefer a certain configuration, which spontaneously breaks the chiral symmetry. According to Goldstone's theorem, when a continuous symmetry is spontaneously broken, there should be massless particles associated with the broken symmetry. These particles are called Goldstone bosons. In the case of chiral symmetry breaking, the pions are the pseudo-Goldstone bosons. They arise because the chiral symmetry is spontaneously broken, and although they are not strictly massless, they have a very small mass compared to other hadrons like protons and neutrons. [Smit'2023]

Light quarks interact through potentials generated by the exchange of pseudoscalar Goldstone bosons (π) and their chiral partner (σ):

$$V_\chi = V_\sigma(r_{ij}^\rightarrow) + V_\pi(r_{ij}^\rightarrow) \quad (5.5)$$

where

$$V_\sigma(r_{ij}^\rightarrow) = \frac{-g_{ch}^2}{4\pi} \frac{\Lambda^2}{\Lambda^2 - m_\sigma^2} m_\sigma \left[Y(m_\sigma r_{ij} - \frac{\Lambda}{m_\sigma}) Y(\Lambda r_{ij}) \right] \quad (5.6)$$

$$\begin{aligned} V_\pi(r_{ij}^\rightarrow) = & \frac{g_{ch}^2}{4\pi} \frac{m_\pi^2}{12m_i m_j} \frac{\Lambda^2}{\Lambda^2 - m_\pi^2} m_\pi \left[Y(m_\pi r_{ij} - \frac{\Lambda^3}{m_\pi^3}) Y(\Lambda r_{ij}) \right] \vec{\sigma}_i \cdot \vec{\sigma}_j \\ & + \left[H(m_\pi r_{ij}) - \frac{\Lambda^3}{m_\pi^3} H(\Lambda r_{ij}) \right] S_{ij}^2(\vec{\tau}_i \cdot \vec{\tau}_j) \end{aligned} \quad (5.7)$$

$\frac{g_{ch}^2}{4\pi}$ is the chiral coupling constant, m_i are the masses of the constituent quarks, $\Lambda \sim \Lambda_{\text{QCD}}$, $Y(x) = \frac{e^{-x}}{x}$ is the standard Yukawa function, $H(x) = (1 + \frac{3}{x} + \frac{3}{x^2})Y(x)$, $S_{ij} = 3(\vec{\sigma}_i \cdot \vec{r}_{ij})(\vec{\sigma}_j \cdot \vec{r}_{ij})\vec{\sigma}_i \cdot \vec{\sigma}_j$ is the quark tensor operator. Instead perturbative QCD effects are taken into account through the one-gluon-exchange (OGE) potential

$$V_{OGE}(r_{ij}^{\vec{r}}) = \frac{\alpha_s}{4} \vec{\lambda}_i^c \cdot \vec{\lambda}_j^c \left[\frac{1}{r_{ij}} - \frac{1}{4} \left(\frac{1}{2m_i^2} + \frac{1}{2m_j^2} + \frac{2\vec{\sigma}_i \cdot \vec{\sigma}_j}{3m_i m_j} \right) \frac{e^{-r_{ij}/r_0}}{r_0^2 r_{ij}} \frac{3S_{ij}}{4m_i m_j r_{ij}^3} \right] \quad (5.8)$$

where \vec{c} are the SU(3) color matrices, $r_0 = \hat{r}_0/\nu$ is a flavor-dependent regularization scaling with the reduced mass ν of the interacting pair, and α_s is the scale-dependent strong coupling constant given by:

$$\alpha_s(\nu) = \frac{\alpha_0}{\ln[(\nu^2 + \mu_0^2)/\gamma_0^2]} \quad (5.9)$$

$\alpha_0=2.118$, $\mu_0 = 36.976$ Mev and $\gamma_0=0.113$ fm^{-1} . the equation 5.9 give rise $\alpha_s \sim 0.54$ for light quark and $\alpha_s \sim 0.43$ for uc pairs. The table resume all the parameter 5.1

$m_{u,d}$ (MeV)	313	$g_{ch}^2/4\pi$	0.54
m_c (MeV)	1752	m_σ (fm^{-1})	3.42
\hat{r}_0 (MeV fm)	28.170	m_π (fm^{-1})	0.70
μ_c (fm^{-1})	0.70	Λ (fm^{-1})	4.2
b (fm)	0.518	a_c (MeV)	230

Table 5.1: The table summarizes the typical values of the parameters present in the previous equation.

Finally, any model imitating QCD should incorporate confinement. Although it is a very important term from the spectroscopic point of view, it is negligible for the hadron-hadron interaction. Lattice QCD calculations suggest a screening effect on the potential when increasing the interquark distance which is modeled here by.

$$V_{CON}(r_{ij}^{\vec{r}}) = -\alpha_c(1 - e^{-\mu_c r_{ij}}) \vec{\lambda}_i^c \cdot \vec{\lambda}_j^c \quad (5.10)$$

The figures 5.1 shows the different diagrams contributing to the charmed baryon-nucleon interaction. The first type of interaction, visible in (a) and (b), is mediated by the exchange of a boson between light quark or between a light and heavy flavor. The second one instead take in account also the exchange of the identical light quark (c) and (d). The second possibility correspond to short range that contain one-gluon exchange contributions that are also missed in hadronic models.

A numerical simulation of the potential is described in ?? performed with lattice QCD with lattice spacing $a=0.0907(13)$ fm and a physical lattice size of $L_a=2.902(42)$ fm. In order to see the quark mass dependence of the potentials, the members of the study had employed three ensembles of gauge configurations. The hopping parameters of these ensembles are $\kappa_{ud}=0.13700$ (Ensemble 1), 0.13727 (Ensemble 2), 0.13754 (Ensemble 3) for u, d-quarks. The figure 5.3 show the λ_c N central potential in the 1_0^S channel for each ensemble with different mass considered for the pion. For Ensemble 1 $m_\pi \sim$

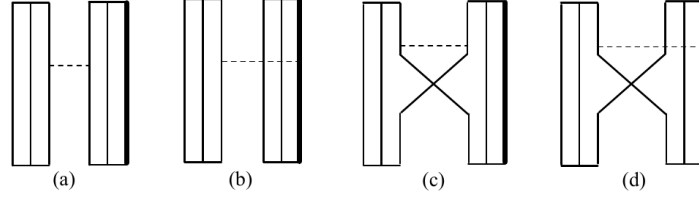


Figure 5.2: The vertical solid lines represent a light quark, u or d. The vertical thick solid lines represent the charm quark. The dotted horizontal lines stand for the exchanged boson. (a) Interaction between two light quarks. (b) Interaction between the heavy and a light quark. (c) Interaction between two light quarks together with the exchange of identical light quarks. (d) Interaction between the heavy and a light quark together with the exchange of identical light quarks.

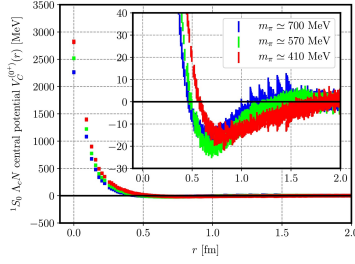


Figure 5.3: The figure show $\Lambda_c N$ central potential in the $1S_0$ channel for each ensemble. The potential is calculated for $m_\pi \approx 700$ MeV case (Blue), for $m_\pi \approx 570$ MeV case (Green) and for $m_\pi \approx 410$ MeV case (Red).

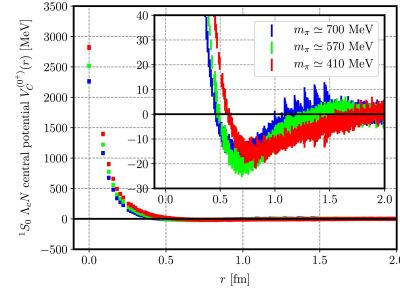


Figure 5.4: The figure show $\Lambda_c N$ central potential in the $3S_0$ channel for each ensemble. The potential is calculated for $m_\pi \approx 700$ MeV case (Blue), for $m_\pi \approx 570$ MeV case (Green) and for $m_\pi \approx 410$ MeV case (Red).

700 MeV, $m_\pi \sim 570$ MeV for Ensemble 2 and 410 MeV for Ensemble 3. They found a repulsive core at short distances ($r \lesssim 0.5$ fm) and an attractive one for intermediate distances ($0.5 \lesssim r \lesssim 1.5$ fm). They discovered also that the height of the repulsive core increases and the minimum of the attractive pocket shifts outward, as u, d quark masses decrease. A variation of the repulsive core against u, d quark masses may be explained by the fact that the colour magnetic interaction is proportional to the inverse of the constituent quark mass. The same operation has also been done with a $\Lambda_c N$ system with $J^P = 1^+$ obtaining the result visible in figure 5.4, the result is similar to the one in $1S_0$ channel except at short distance ($r \lesssim 0.5$ fm) but in both cases the attractive potential is weaker than the $\Lambda_c N$ system.

The weaker potential than $\Lambda_c N$ could be explained from following facts:

- The long-range contribution is expected to be caused by the K meson exchange for ΛN interaction. In the system, however, the K meson (strange quark) exchange is replaced by the D meson (charm quark) exchange, and this contribution is highly suppressed due to the much heavier D meson mass than the K meson mass.
- The one-pion exchange in the transition is considered to give a sizable contribution to the effective ΛN interaction. In the system, however, this contribution is expected to be suppressed due to the large mass

difference between $\Lambda_c N$ and $\Sigma_c N$

If no meson exchanges were considered, the S wave phase shifts of the $\Lambda_c N$ system are very similar to the corresponding NN scattering. In both partial waves one obtains typical hard-core phase shifts due to the short-range gluon and quark-exchange dynamics. However, the hard-core radius in the spin-singlet state is larger than in the spin-triplet one leading to a more attractive interaction in the spin-triplet partial wave due to a lower short-range repulsion. In fact, the hard cores caused by the color magnetic part of the OGE potential have been calculated obtaining 0.35 fm for the spin-triplet state and 0.44 fm for the spin-singlet one.

5.0.3 Potential energy

5.0.4 Possible Λ_c supernuclei

One of the most interesting applications of the charmed baryon-nucleon interaction is the study of the possible existence of charmed hypernuclei. Since the Λ_c interaction is dominated by the spin-independent central force, as we discussed in the previous section, the spectrum of hypernuclei, if they exist, would probably can be approximated by the following single-folding potential defined by

$$V_f(\vec{r}) = \int d^3 r' \rho_A(\vec{r}') V_{\Lambda_c N}(\vec{r} - \vec{r}') \quad (5.11)$$

where $\rho_A(\vec{r})$ correspond to ne nuclear density corresponding with the atomic number A and $V_{\Lambda_c N}$ stands for the two body spin-independent central potential of the Λ_c system. The study described assumed,

$$\rho_A(\vec{r}) = \rho_0 \left[1 + e^{\frac{r-c}{a}} \right] \quad (5.12)$$

where the parameters employed ρ_0 , c, a are the same used for described spherical nuclei. They test the equation with different set of parameter taking the value assumed in the following nuclei 12^C , 28^Si , 40^Ca , 58^Ni and 208^Pb . With the following potential they calculate the binding energy for Λ_c hypernuclei by the Gaussian expansion method. The result is shown in figure 5.5. As expected the binding increases as the atomic number increases. Furthermore, as the potential approaches to the physical one (as the u, d quark masses decrease toward physical values), the binding energy increases. These results suggest that hypernuclei may exist, if their binding energy is larger than the Coulomb repulsion energy described by??.

It's interesting to confront energy expectation taking into account also the Culomb repulsion, the result is reported in figure 5.6. It's possible to see that only the system with lower atomic number could eventually exist.

The binding energy of Λ_c hypernuclei has been analyzed in ?? using the HAL QCD for $m_\pi = 410$ MeV.

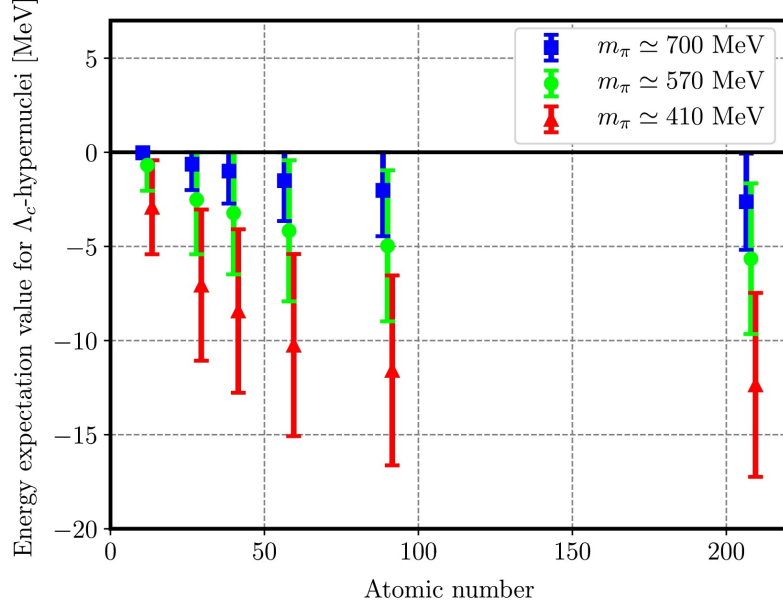


Figure 5.5: The figure show the binding energy in symmetric nuclei with the parameter assumed for each atomic number for each ensemble. The binding energies are calculated from the folding potentials for Λ_c hypernuclei by using the Gaussian expansion method. The folding potentials are constructed from the spin-independent central potential of the $\Lambda_c N$ system

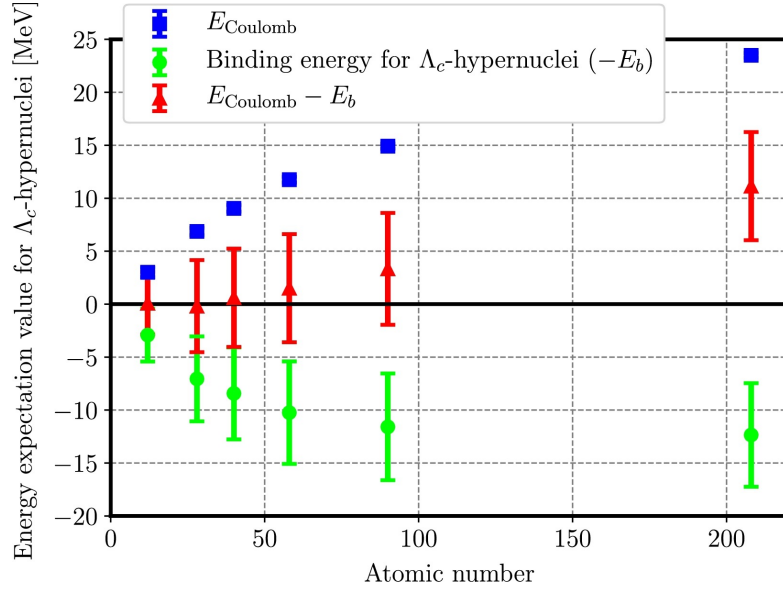


Figure 5.6: The figure show the expectation value of folding potential for Coulomb force in Λ_c hypernuclei (Blue). The expectation values are calculated from the binding solution of the Λ_c hypernuclei for Ensemble 3 ($m_\pi \approx 410$ MeV). For comparison, the binding energy of Λ_c hypernuclei (Green) and sum of them (Red) are also plotted.

Chapter 6

ALICE

.0.1 Cooper-Frye

We start with the proof that $dyp_{\perp}dp_{\perp}d\phi_p = dym_{\perp}dm_{\perp}d\phi_p$, in fact $m_{\perp} = \sqrt{m^2 + p_{\perp}^2}$ so $\frac{dm_{\perp}}{dp_{\perp}} = \frac{p_{\perp}}{\sqrt{m^2 + p_{\perp}^2}} = \frac{p_{\perp}}{m_{\perp}}$ and the result follow immediately.

For the other equation starting from 4.4 and inserting 4.1 one get

$$\frac{dN_i}{dym_{\perp}dm_{\perp}d\phi_p} = \frac{g_i}{(2\pi)^3} \sum n = 1^{\infty}(\pm)^n \int d^2r_{\perp} \tau_f e^{n\mu_i/T} e^{n\gamma_{\perp} \vec{v}_{\perp} \cdot \vec{p}_{\perp}} x \int_{-\infty}^{+\infty} d\eta (m_{\perp} \cosh(y - \eta) - \vec{p}_{\perp} \cdot \vec{v}_{\perp}) \quad (1)$$

Where the modified Bessel function enters the game. The azimuthal integral can thus be done analytically

$$\frac{dN_i}{dym_{\perp}dm_{\perp}} = \frac{g_i}{(2\pi)^3} \sum n = 1^{\infty}(\pm)^n \int dr_{\perp} \tau_f e^{n\mu_i/T} \left(m_{\perp} K_1(nm_{\perp} \frac{\gamma_{\perp}(\vec{r}_p \cdot \vec{p})}{T(\vec{r}_p \cdot \vec{p})}) I_0(n \frac{p_{\perp} v_{\perp} \gamma_{\perp}}{T}) - p_{\perp} \frac{\partial \tau}{\partial r_{\perp}} \right) \quad (2)$$

and finally defying $v_{\perp} = \tanh \rho$ one get

$$\frac{dN_i}{dy m_{\perp} dm_{\perp} d\phi_p} = \frac{g_i}{\pi} \int_0^{\infty} r_{\perp} dr_{\perp} n_i(r_{\perp}) \left[m_{\perp} K_1 \left(\frac{m_{\perp} \cosh(\rho(r_{\perp}))}{T(r_{\perp})} \right) I_0 \left(\frac{p_{\perp} \sinh(\rho(r_{\perp}))}{T(r_{\perp})} \right) - p_{\perp} \frac{\partial \tau}{\partial r_{\perp}} \right] \quad (3)$$